Minerals Engineering 61 (2014) 113–120

Contents lists available at ScienceDirect

Minerals Engineering

journal homepage: www.elsevier.com/locate/mineng

Biologically enhanced degassing and precipitation of magnesium carbonates derived from bicarbonate solutions

Timothy K. Oliver, Bogdan Z. Dlugogorski *, Eric M. Kennedy

Priority Research Centre for Energy, Faculty of Engineering and Built Environment, ATC Building, The University of Newcastle, Callaghan, NSW 2308, Australia

ARTICLE INFO

Article history:
Available online 3 December 2013

Keywords:
Accelerated mineral carbonation
Nesquehonite precipitation
Degassing
Carbonic anhydrase
Alkalisation

ABSTRACT

This contribution reports the results of batch and semibatch experiments involving bubbling of nitrogen in aqueous solutions of magnesium bicarbonate, with and without the addition of either carbonic anhydrase (CA) or *Scenedesmus alga* to the solution. Precipitation of nesquehonite occurred during both an accelerated degassing of CO_2 induced by sparging small nitrogen bubbles (representative diameter of 20 μm), and during slow degassing engendered by introducing large nitrogen bubbles (representative diameter of 5 mm). The response of the system during low rates of degassing closely approached quasi-thermodynamic predictions, which permitted an estimation of the level of supersaturation of nesquehonite, prior to the onset of precipitation. Small bubbles and CA significantly increased rates of degassing and indirectly the production of nesquehonite, as the rate of degassing can limit the precipitation process. The response of the system during rapid rates of degassing, prior to precipitation, was not entirely consistent with quasi-thermodynamic predictions. During precipitation, higher rates of degassing produced similar alkalisation and precipitation trends to that observed for lower rates of degassing. Our results agree with the formation of travertine deposits in nature, where the degassing of solutions enriched with inorganic carbon, and enhanced alkalisation by microorganisms, have been shown to influence carbonate formation. The results demonstrate a catalytic effect of CA on the rate limiting carbonate reactions, increasing CO_2 exchange between nitrogen and water, and indirectly accelerating the precipitation of carbonates for a system controlled by rate of degassing. The results of this study have applications to large-scale storage of CO_2 by mineralisation.

1. Introduction

The evasion or degassing of carbon dioxide (CO_2) from mineral solutions enriched in inorganic carbon represents a promising approach to mineral carbonation. For a solution rich in mineral ions, degassing causes the solution pH to increase and leads to elevated mineral saturation indices and mineral precipitation. The process of degassing of CO_2 is fundamentally a kinetic phenomenon driven by the difference in chemical potential of CO_2 between the bulk solution and that of the gas–liquid interface. That is, the chemical behaviour of the system depends on the concentration of carbonate species in the bulk solution and on mass transfer of CO_2 across the liquid–gas interface. The concentration of carbon species in the bulk solution decreases as CO_2 degassing of the solution progresses.

Microalgae and in particular carbonic anhydrase (CA), an enzyme produced by microalgae and living organisms more generally, have been implicated in the precipitation of carbonates in nature (Liu, 2001; Liu et al., 2010; Sondi and Mladen, 2010). The precipitation mechanism is controlled kinetically by the rate of CO_2 removal from the system, and thermodynamically by pH; the latter elevated through the cellular consumption, by the microalgae, of aqueous CO_2 and bicarbonate, HCO_3^-. Microalgae extracellular CA is the catalytic component in the carbon concentrating mechanisms (CCM) used to promote uptake of carbon into the cell needed for growth and metabolism of the algae. In instances, for example in the formation of travertine deposits, both microorganisms and degassing of solutions enriched with inorganic carbon, have been shown to influence carbonate formation (Pentecost, 2005). CA has been demonstrated as an activator in the accelerated weathering of carbonate rocks, and the enzyme has been previously shown to increase rates of CO_2 exchange between air and sea water, and intensify rates of precipitation of carbonates by way of catalysing rate limiting carbonate reactions (Berger and Libby, 1969; Liu, 2001; Dreybrodt et al., 1997).

This study investigates the degassing of carbon enriched solutions, in a situation analogous to natural mechanisms, and the enhancement of the degassing and precipitation mechanisms through incorporation of CA and microalgae in the reacting system to increase the rate of production of carbonate. The study explores batch and semibatch operations.

* Corresponding author. Address: School of Engineering and Information Technology, Murdoch University, 90 South Street, Murdoch, Western Australia 6150, Australia. Tel.: +61 8 9360 6770.
E-mail address: B.Dlugogorski@murdoch.edu.au (B.Z. Dlugogorski).

0892-6875/$ - see front matter © 2013 Elsevier Ltd. All rights reserved.
http://dx.doi.org/10.1016/j.mineng.2013.11.003

2. Materials and methods

2.1. Materials

Solutions for batch and semibatch experiments were prepared with ultrapure deionised water with electrical resistivity of 18.2 MΩ/cm and reagent grade magnesium sulfate heptahydrate ($MgSO_4{\cdot}7H_2O$) and sodium bicarbonate ($NaHCO_3$). Glass bottles contained the solutions for batch experiments, and polyethylene bottles for the semibatch experiments. Gaseous nitrogen (N_2) used for aeration was discharged into the reactor through either a 2 μm aperture stainless steel air diffuser or directly through 4 mm ID silicone tubing. A thermostatically controlled water bath (Axyos Technologies, Model w10) housed bottles containing the solutions for batch and semibatch experiments. Mini variable flow peristaltic pumps (VWR and Control Company) fed reagent solutions to the reactor for the semibatch experiments.

Supplements to chemical reagents used in preparing the test solutions included bovine carbonic anhydrase (CA) (Worthington Biochemical, carbonic anhydrase from bovine erythrocytes, dialysed, lyophilised powder) and the green freshwater alga *Scenedesmus* (species 005; Australian Water Quality Centre). Cellulose fibre filter pads (0.2–0.5 μm) served to filter algal solutions. Submersible white LED lights (Nelson Industries, MGL540LED) illuminated algae supplemented solutions. An illuminometer (Kyoritsu, Model 5200) facilitated light intensity measurements. A haemocytometer (Neubauer-improved bright-lined haemocytometer (Superior Marienfeld)) enabled a cell count of algal solutions.

A pH glass electrode (Hanna HI 1131) recorded proton activity in the experimental solutions, with the electrode calibrated at working temperature with commercial buffer solutions. Measurements were logged with 'DataTaker' (505 Series 2 Data Logger) data acquisition hardware. Solutions at the end of each experiment were filtered using Whatman Grade 1 paper filters and then using Millex GP 0.22 μm syringe driven filters. A Varian 715-ES inductively coupled plasma–optical emission spectrometer (ICP-OES) provided the elemental analysis of magnesium (Mg) present in filtered samples (0.22 μm) of the test solutions. X-ray powder diffraction (XRPD) with a Philips X'Pert Pro multipurpose diffractometer using Cu Kα radiation in the range of 5° to 90° 2θ, with a step size of 0.008° and collection time of 42 s $step^{-1}$, were deployed for the identification of the mineral phase in precipitates. The gaseous vent stream from the solution passed through a membrane separator (Genie Model 170–005-SS) prior to its CO_2 concentration being measured with a micro gas chromatograph (Varian 4900 micro GC with PoraPLOT Q column with column temperatures of 60 °C and injection time of 40 ms). Initial volumes of the vented N_2 stream from the experiments were collected using sample bags (SKC FlexFoil PLUS) for subsequent analysis using the micro GC.

2.2. Methods

Batch and semibatch experiments involved bubbling of N_2 in aqueous solutions of magnesium sulfate ($MgSO_4$) and sodium bicarbonate ($NaHCO_3$). The preparation of the $MgSO_4$ solutions using magnesium sulfate heptahydrate ($MgSO_4{\cdot}7H_2O$) accounted for the hydrated nature of this compound in establishing molar concentrations of the $MgSO_4$ solutions; typically 0.1 M $MgSO_4$ and 0.1 M $NaHCO_3$. The temperature of the thermostatically controlled water bath housing the bottle reactors was set to 30 °C for all batch and semibatch experiments. Gaseous N_2 at a preset rate flowed to the reactor containing the test solutions with N_2 discharged into the solution at the base of the reactor through an air diffuser or directly through tubing. The period for all batch experiments was 24 h and for semibatch experiments 4 h.

Table 1 provides a summary of experimental conditions for the batch experiments. Prior investigations, during which reported trends were clearly evident, permitted establishment of appropriate experimental conditions for the batch reactor.

Two of the batch and one of the semibatch experiments exploited CA at a concentration of 0.5 μM and 0.25 μM, respectively. The selection of a 0.5 μM CA concentration corresponded to that used in previous research (Dreybrodt et al., 1997), and the application of a 0.25 μM strength CA solution for semibatch experiments allowed for a prefatory assessment of the effect of varying CA concentration. Semibatch experiments comprised the continual addition of reagent solutions (0.5 M $MgSO_4$ and 0.34 M $NaHCO_3$ to result in molar dosing rates of 1.1×10^{-5} mol s^{-1} and 2.3×10^{-5} mol s^{-1}, respectively) as separate streams into the reactor. The reagent streams entered into an initial batch solution of the same chemical composition as that deployed for the batch experiments.

We also completed a batch experiment using *S. alga*. The growth medium for the alga comprised demineralised water supplemented with soluble plant nutrient. Cultures grew at air-equilibrated levels of CO_2 at ambient laboratory conditions under a lighting level of 1000 lux. Filtration of aliquots of culture through cellulose fibre filter pads, and rinsed with ultrapure deionised water prior to harvest, provided a concentrated algal inoculum. The filtered and rinsed microalgae of paste-like consistency were then added to a solution that comprised only $MgSO_4{\cdot}7H_2O$ reagent. Submersible lighting illuminated the test solution at a level of 10,000 lux. A diluted sample (5:1) of the test solution allowed for an algal cell count. The inoculated solution was then bubbled with CO_2 and subsequently purged with gaseous N_2 under ambient conditions in order to promote CA production by the microalgae. Finally, the addition of $NaHCO_3$ reagent resulted in a solution of chemical composition of 0.1 M $MgSO_4$ and 0.1 M $NaHCO_3$. Aeration of the prepared solution using N_2 followed.

Gaseous N_2 at a preset rate flowed to the reactor containing the test solutions, discharging into the solution at the base of the reactor through either the air diffuser or directly through tubing. The former generated small bubbles giving rapid bubbling and an accelerated rate of mass transfer through its large interfacial area, and the latter formed large bubbles resulting in slow bubbling and a diminished rate of mass transfer through reduced interfacial area. Bubbles were photographed and empirically sized and bubble travel times estimated using a digital camera with video capture. Bubble coalescence was evident for N_2 aeration generated by tubing. Fluid depth (bubble travel distance) was approximately 50 mm for the batch experiments and initially 30 mm increasing to 120 mm for the semibatch experiments. Representative bubble diameter, time to traverse 50 mm of fluid depth and rise velocity corresponded to 5 mm, 0.22 s and 0.23 m s^{-1} respectively for tubing, and 20 μm, 0.15 s and 0.33 m s^{-1} respectively for the air diffuser. At the conclusion of each experiment involving the diffuser, we recorded a value of the decreased flow rate of N_2, as a consequence of carbonate build-up in the pores of the diffuser.

We sampled the test solutions at the commencement and conclusion of each experiment, decanting and then filtering them for subsequent analysis. Potentiometric titration of 5 cm^3 or 10 cm^3 aliquots of 0.22 μm filtered samples against standardised 0.01 M sulfuric acid (H_2SO_4) enabled the determination of alkalinity of the samples. ICP-OES analysis afforded determination of Mg balance. Sample bags accumulated the vented gas stream for the first 2 min of degassing, in duplicated experiments, for subsequent analysis using the micro GC. All precipitate, including that which was retained within the reactor, underwent drying under ambient conditions open to atmosphere until attaining stable mass measurements. Mineral phase identification utilised the dried precipitates.

Table 1
Experimental conditions for batch experiments. Note that the N_2 flow rate declined during the experiments with diffuser aeration as a consequence of clogging of the diffuser pores by precipitating carbonates.

Experiment	Initial N_2 flow ($cm^3\ s^{-1}$)	Means of N_2 aeration	Basis solution (Vol. = 180 cm^3)	Temperature (°C)
1	8.5	Diffuser	0.1 M $MgSO_4$ + 0.1 M $NaHCO_3$	30
2	8.5	Diffuser	0.1 M $MgSO_4$ + 0.1 M $NaHCO_3$ + 0.5 μM CA	30
3	8.5	Diffuser	0.1 M $MgSO_4$ + 0.1 M $NaHCO_3$ + *Scenedesmus alga* (1.1×10^7 cells cm^{-3})	30
4	8.5	Tubing	0.1 M $MgSO_4$ + 0.1 M $NaHCO_3$	30
5	8.5	Tubing	0.1 M $MgSO_4$ + 0.1 M $NaHCO_3$ + 0.5 μM CA	30
6	15	Tubing	0.1 M $MgSO_4$ + 0.1 M $NaHCO_3$	30
7	15	Tubing	0.1 M $MgSO_4$ + 0.1 M $NaHCO_3$ + 0.5 μM CA	30

The elemental carbon (C) balance for each experiment relied on (i) estimates of vented CO_2 concentrations from micro GC measurements, (ii) N_2 flow rate, (iii) known initial solution concentrations, (iv) discrete alkalinity measurements, (v) identification of the mineral phase, and (vi) mass measurement of precipitate. The elemental Mg balance followed from (i) initial solution concentrations, (ii) ICP-OES measurements of residual solutions for each experiment, (iii) mineral phase identification of the precipitate, and (iv) its mass determination.

3. Results and discussion

All degassing experiments exhibited a similar pH trend that can be categorised into three distinct phases (shown by reference to Experiment 1 and as illustrated in Fig. 1). Phase 1 represents the alkalisation of the solution prior to onset of carbonate precipitation. During this phase, the solution rapidly degasses, prompting supersaturation of minerals. Degassing is a form of decarbonation of the solution, with the decarbonation mechanism described by Wolf-Gladrow and Riebesell, as well as Gavis and Ferguson (Gavis and Ferguson, 1975; Wolf-Gladrow and Riebesell, 1997). The gas–liquid interface of the bubble forms two diffusive boundary layers (DBLs). In the thin film model of gas exchange, diffusion-mediated films on either side of the gas–liquid interface control overall mass transfer (Stumm and Morgan, 1996; Johnson, 2010). In the aqueous-side DBL, diffusion and aqueous carbonate reactions take place, whereas only diffusion occurs in the gas-side DBL.

The difference in CO_2 chemical activity between the bulk solution and the gas phase can result in changes in the activities of carbonate species within the aqueous-side DBL.

Both the process of diffusion and carbonate system reactions determine the concentration of carbonate species in the aqueous-side DBL. Under a steady state condition, the rate of removal of inorganic carbon from the system equals the rate of resupply through diffusive transport and chemical reactions (Wolf-Gladrow and Riebesell, 1997). The loss of one mole of CO_2 from solution entails consuming one mole of HCO_3^- and producing one mole of OH^-, progressively transforming the alkalinity of the system from one based initially on HCO_3^- to that based predominantly on OH^- and CO_3^{2-}.

The initial phase (Phase 1) also comprises the crystallisation induction period; that is, the time required for the formation of stable carbonate nuclei (Söhnel and Mullin, 1988). The end of the first phase coincides with the onset of precipitation as indicated by a peak in pH prior to a measurable drop in pH. For the second phase, mineral precipitation proceeds until the concentration of Mg and carbonate ions are diminished to a point whereby further nucleation is unviable (Emmanuel and Ague, 2011). The final or third phase represents the further alkalisation of the solution until the solution approaches a maximum pH. During this final phase, and discounting the influence of moisture loss from the system, the system moves towards a steady state condition. Under this condition, the inorganic carbon content of the solution subsides to the point where CO_2 from the atmosphere (as the solution is open to local atmosphere) provides an influx of CO_2 to the solution which is then removed through the N_2 aeration medium. A balance between the CO_2 efflux facilitated by the N_2 aeration medium and CO_2 influx from local atmosphere produces this state. Additionally, the final phase involves establishment of a steady state condition between the aqueous species and also between the aqueous and solid phases, such as nesquehonite. During experiments, we observed no transformation of the precipitating phase, nesquehonite, to less hydrated carbonate phases.

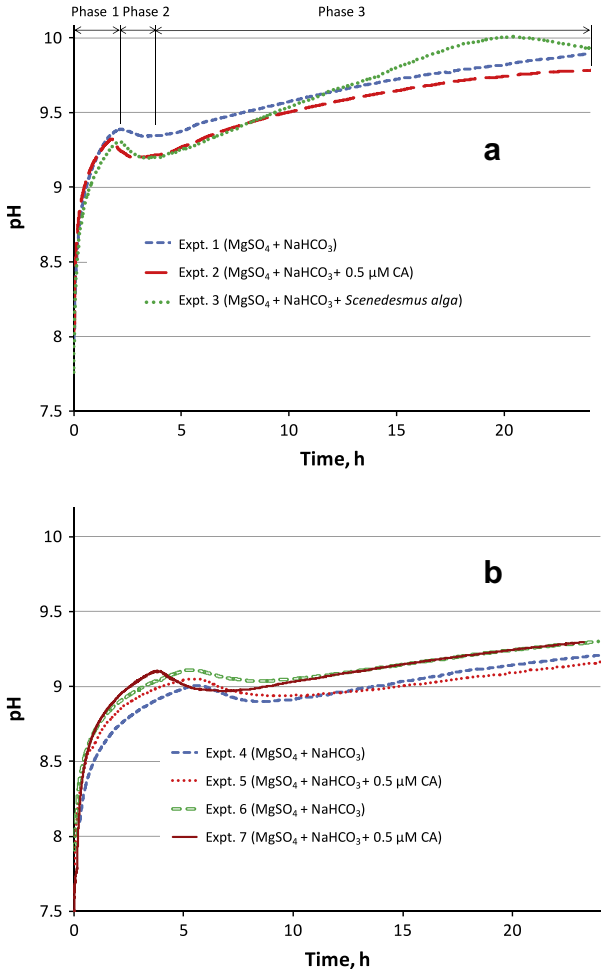

Fig. 1. Induced trends in pH: (a) batch, small bubbles, generated by diffuser; (b) batch, large bubbles, produced by tubing.

Eq. 1 represents the overall stoichiometry of nesquehonite precipitation; the precipitated phase identified in this study (Zeebe and Wolf-Gladrow, 2001; Pentecost, 2005). Here, we consider nesquehonite as a single-component carbonate, whose formation

follows the same reaction pattern as that described for calcite (Dreybrodt, 2004; Chou et al., 1989).

$$Mg^{2+}_{(aq)} + 2HCO^{-}_{3(aq)} + 3H_2O \rightarrow MgCO_3 \cdot 3H_2O_{(s)} + CO_{2(aq)} + H_2O \quad (1)$$

The PWP (Plummer, Wigley and Parkhurst) model for dissolution/precipitation, given by Eqs. (2)–(4), depicts forward and reverse reactions that operate in the process.

$$MgCO_3 \cdot 3H_2O_{(s)} + H^{+}_{(aq)} \rightleftharpoons Mg^{2+}_{(aq)} + HCO^{-}_{3(aq)} + 3H_2O \quad (2)$$

$$MgCO_3 \cdot 3H_2O_{(s)} + H_2CO^{\circ}_{3(aq)} \rightleftharpoons Mg^{2+}_{(aq)} + 2HCO^{-}_{3(aq)} + 3H_2O \quad (3)$$

$$MgCO_3 \cdot 3H_2O_{(s)} \rightleftharpoons Mg^{2+}_{(aq)} + CO^{2-}_{3(aq)} + 3H_2O \quad (4)$$

The rates of these reactions depend on pH. The derivation of molar flux for the precipitating nesquehonite stems from this reaction set. The overall stoichiometry for precipitation at the mineral surface however must apply (cf. Eq. 1) and consequently rapid rates of precipitation may result in reduced pH (cf. Eq. 2).

CA acts to enhance carbonate reactions, specifically the reversible HCO^{-}_{3} dehydroxylation and H_2CO_3 dehydration reactions, driving them to the equilibrium. These reactions are represented in Eqs. (5) and (6).

$$HCO^{-}_{3} \rightleftharpoons CO_{2(aq)} + OH^{-}_{aq} \quad (5)$$

$$HCO^{-}_{3(aq)} + H^{+}_{(aq)} \rightleftharpoons H_2CO_{3(aq)} \rightleftharpoons CO_{2(aq)} + H_2O \quad (6)$$

Dreybrodt and co-workers, in experiments with supersaturated solutions containing CA, found rates of precipitation of calcite increased by a factor of up to 15 (Dreybrodt et al., 1997). Additionally transport of the dissolved species to and from the mineral surface can become a rate limiting step for precipitation (Plummer et al., 1978; Koutsoukos et al., 2007). Increased rates of alkalisation induce rapid attainment of mineral supersaturation and higher supersaturation levels.

In the case of dehydroxylation, the resultant evasion of CO_2 from the bulk solution leads directly to solution alkalisation, whereas the dehydration reaction, predominating at lower pH, consumes H^+ thereby also causing an elevation in solution pH. The lower rate of alkalisation, through the slow rate of degassing from large bubbles (generated via tubing), compared to fast alkalisation through the rapid rate of degassing from small bubbles (generated via diffuser), follows from significantly reduced interfacial area and hence reduced mass transfer of CO_2. The actual alkalisation effect can be directly measured by quantitating the loss of CO_2 during degassing.

Progressive CO_2 loss during each degassing experiment was established from micro GC measurements. Fig. 2 illustrates typical trends in the rate of degassing (Experiments 2 and 4) and the cumulative CO_2 loss for each of the batch experiments. CA increases the rate of alkalisation and the amount of CO_2 degassed both in experiments with small (20 μm) and large (5 mm) bubbles. Plots of degassing in Fig. 2 have a truncated vertical scale for clarity. Measured concentrations of CO_2 after 60 s amounted to 35,000 ppmv and 6200 ppmv in the vented stream, for Experiments 2 and 4, respectively. CA was also found to accelerate the onset of precipitation.

In the case involving *S. alga*, the trend represents not only the effect of CA but also the continuing growth of the alga in solution. In this instance, we see an accelerated rate of alkalisation, again corroborated by the relative decrease in CO_2 concentration in the vented stream, more rapid increase in pH following the initial phase of precipitation, and a subsequent decline in solution pH later in the experiment (cf. Fig. 1).

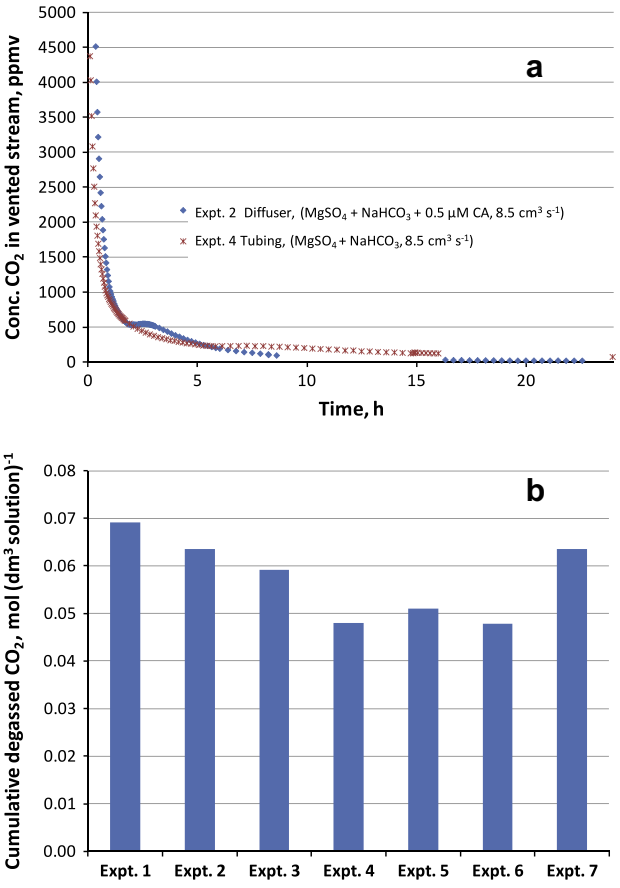

Fig. 2. (a) Concentration and (b) cumulative amount of CO_2 in vented stream, illustrating degassing trends; based on batch Experiments 2 and 4.

The degassing of the solution is fundamentally a kinetic process. Although the solution is in rapid transition, the pH and carbon loss results show that a quasi-thermodynamic approximation is suitable to interpret results during degassing, prior to precipitation, for slower rates of CO_2 degassing. Nesquehonite is not in equilibrium with other species as there is a kinetic barrier to its precipitation. However, among other species, equilibrium is established. The slow removal of CO_2 allows quasi-equilibrium to be established among the chemical species remaining in the solution, affording prediction of pH as a function of CO_2 loss from solution.

Fig. 3 presents plots of the amount of CO_2 degassed from solution and the resultant pH of the system predicted from PHREEQC thermodynamic software (Parkhurst and Appelo, 1999), compared with the measurements of Experiments 1 to 7. The quasi-thermodynamic calculations involved computation of the equilibrium in the aqueous phase only; i.e., with no solid phase present. The experimental measurements show a close correlation with the results of quasi-thermodynamic calculations for slow rates of degassing. Rapid degassing achieved through the generation of small bubbles from the diffuser and the application of CA produce rates of alkalisation below those expected from quasi-thermodynamic calculations. Hence, these two systems are far from equilibrium. We also exploited PHREEQC thermodynamic software (Parkhurst and Appelo, 1999) to estimate the extent of supersaturation of the carbonate phase; given by $S = IAP/K_{SP}$, where *IAP* equates to the ion activity product and K_{SP}, the solubility product constant of nesquehonite, $MgCO_3{\cdot}3H_2O$, established from the PRONS thermodynamic database (Helgeson, 1988). The results yielded a near-linear dependence of nesquehonite saturation on the cumulative amount of CO_2 removed from the solution, as illustrated in Fig. 4.

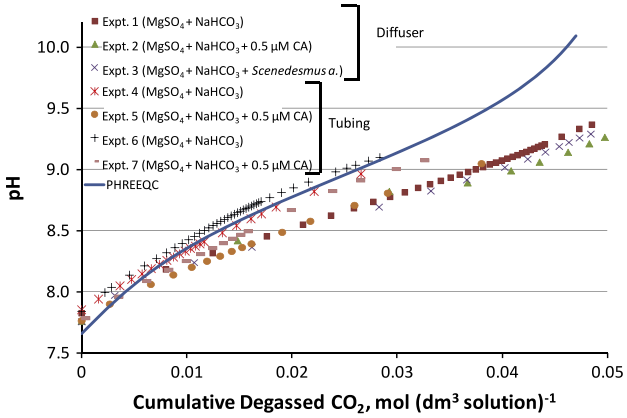

Fig. 3. The effect of the cumulative CO_2 degassed from solution on resultant pH of the solution; comparison of experimental measurements with thermodynamic predictions showing departure for rapid bubbling/degassing cases.

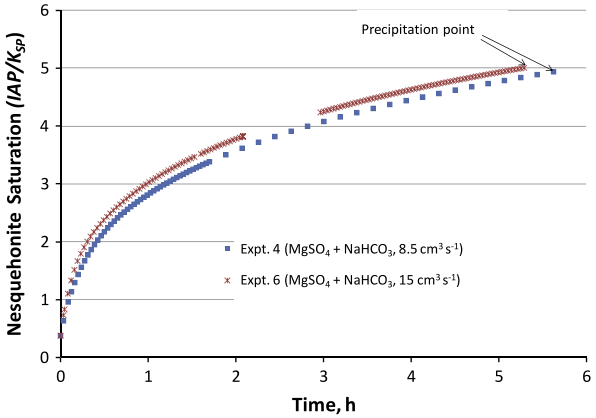

Fig. 5. Slow build-up of supersaturation of nesquehonite, as a consequence of degassing the bicarbonate solution with large bubbles.

The relationship between nesquehonite saturation and the cumulative amount of CO_2 removed from the solution was used to illustrate a time evolution of mineral supersaturation for experiments exhibiting quasi-thermodynamic behaviour, as shown in Fig. 5 for Experiments 4 and 6. In a quasi-thermodynamic system, most chemical species exist in thermodynamic equilibrium among themselves, but a kinetic barrier prevents the remaining species (such as nesquehonite) to attain equilibrium, leading to build-up of supersaturation prior to the initiation of precipitation. These experiments employed large bubbles that caused slow removal of CO_2. Slightly faster removal of CO_2 by N_2 flowing at 15 $cm^3\ s^{-1}$ rather than at 8 $cm^3\ s^{-1}$ induced earlier precipitation; see the endpoints of the curves drawn in Fig. 5. Under this scenario of slow CO_2 removal, the precipitation of nesquehonite commences once its supersaturation reaches a value of approximately 5, using the PRONS database (Helgeson, 1988) for the calculation of the thermodynamic properties of nesquehonite. As moisture loss was not measured progressively during the course of the experiments, it is not accounted for in Fig. 5. However, based on mass measurements of solutions at the end of experiments, we would expect, for example, a 2.6% loss of moisture from the reacting system at the point of precipitation for Experiment 4. Allowing for this extent of moisture loss would result in the supersaturation of nesquehonite to increase from 5.0 to 5.1, at the point of precipitation; i.e., a small effect.

Eqs. (7) and (8) represent the alkalinity (Alk) and dissolved inorganic carbon (DIC), respectively

$$\mathrm{Alk} = [HCO_3^-] + 2[CO_3^{2-}] + 2[MgCO_3^0] + [MgHCO_3^+] + [MgOH^+] + 2[NaCO_3^-] + [NaHCO_3^0] + [NaOH] - [H^+] + [OH^-] \quad (7)$$

$$\mathrm{DIC} = [HCO_3^-] + [CO_3^{2-}] + [MgCO_3^0] + [MgHCO_3^+] + [NaCO_3^-] + [NaHCO_3^0] \quad (8)$$

where brackets represent molar concentrations.

The initial solution composition, measured amount of vented CO_2, measured pH and the known stoichiometry of precipitation, yielded the profiles of the rate and cumulative precipitation for Experiment 4, as illustrated in Fig. 6. This calculation was completed using PHREEQC software (Parkhurst and Appelo, 1999), accounting for various ion pairs and chemical activity coefficients, and taking the aqueous system to be in thermodynamic equilibrium throughout precipitation. This is an approximation, as we have not demonstrated that during precipitation our system approaches the thermodynamic equilibrium. A kinetic model would provide more accurate prediction of the degassing/precipitation behaviour for all experiments, especially those that comprise small bubbles and/or CA, as both approaches engender fast CO_2 removal. Such a model, able to predict degree of supersaturation, will be presented in a subsequent publication.

In Fig. 6a, we observe an accelerating rate of precipitation, a maximum at approximately 2 h, and then a decline. The initial rate relates to the growth of stable carbonate nuclei, a short period of stable rate indicates a rate controlled process, and a decline signifies a substrate limitation.

Other researchers have shown the influence of CA in accelerating precipitation through catalysis of carbonate reactions (Dreybrodt et al., 1997; Mahinpey et al., 2011) that reduced the induction time prior to precipitation (Liu et al., 2005). The indirect effect of CA on the rate of precipitation for the batch degassing process requires an explanation. pH defines the chemical potential difference driving precipitation, which increases with pH; i.e., this is a thermodynamic effect. In the absence of pH buffering, any precipitation lowers the pH of solution in accordance with the overall stoichiometry of the precipitation reaction (cf. Eq. (1)). This thermodynamic behaviour applies irrespective of whether CA operates or not; i.e., CA exerts a kinetic effect on the process. The rate at which CO_2 is removed from solution is dependent on the CO_2 activity in the solution, and the presence of a catalyst, such as CA. However, in the absence of pH buffering, CO_2 removal influences pH. A series of reactions that operate within the system affects the rates of formation and transformation of carbonate species relevant to precipitation and degassing, and this again highlights the advantage of kinetic simulation of the behaviour of the system.

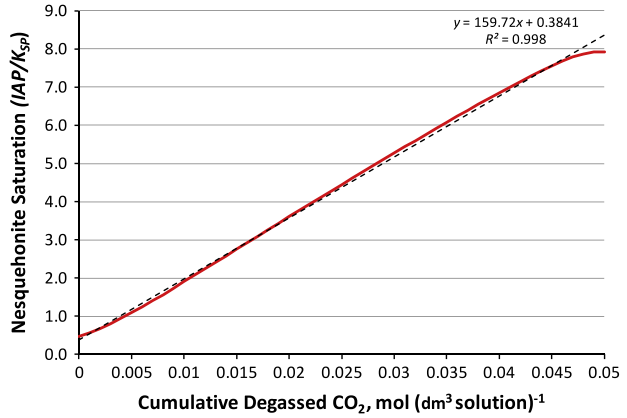

Fig. 4. Modelled nesquehonite saturation versus CO_2 degassed from solution for aqueous phase system and excluding solid phase (carbonate precipitate).

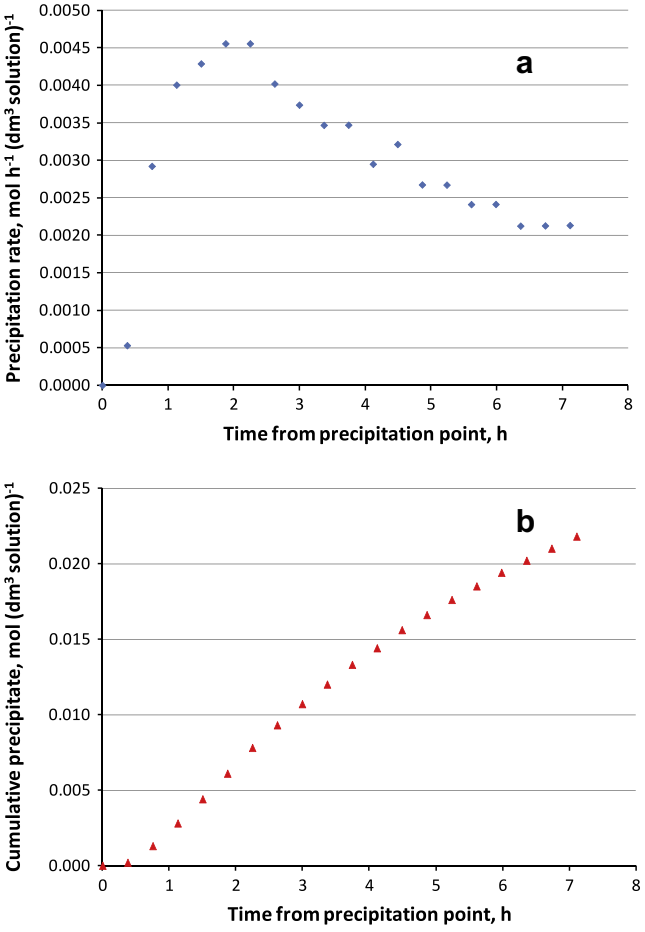

Fig. 6. (a) Bulk precipitation rate and (b) progressive total precipitate for slow rate of CO_2 degassing (Experiment 4); both figures constitute predictions that assume thermodynamic equilibrium during precipitation.

Consequently, although rapid rates of decline in pH, indicative of accelerated precipitation, are evident for cases involving CA and aeration through small bubbles, this effect should be considered in the light of the above comments. More rapid decline in pH during precipitation is not evident for the slower degassing experiment with larger bubbles employing CA. This observation may point to a limitation in the diffusion of CO_2 at the precipitating mineral surface (cf. Fig. 1).

For Experiments 1 to 5, we computed Mg and C elemental balances, requiring determination of the amount of precipitate produced. Sufficient data were unavailable for Experiments 6 and 7 as delay in filtering the residual solutions resulted in secondary precipitation of nesquehonite. For the experiments with the diffuser, aeration experienced declining N_2 flow rates due to clogging of diffuser pores by precipitating carbonates, despite the set N_2 flow rate. For the purpose of completing carbon balances, N_2 flows, as discharged into the reactor, were measured at the conclusion of each experiment and these were 71%, 63% and 43% of the initial flow rate for Experiments 1, 2 and 3 respectively. The rate of CO_2 loss and hence cumulative CO_2 loss from the experiments was adjusted to account for reduced flow of N_2 through the system with adjustment applied from the point of precipitation. DIC calculations for the residual solutions were completed using PHREEQC software (Parkhurst and Appelo, 1999) accounting for C loss from precipitated carbonate and cumulative C loss from CO_2 vented, and Mg loss from precipitated carbonate. Measurement of initial and final solution mass enabled calculation of the amount of water lost from the system during aeration. Percentage mass losses were calculated as approximately 9% for Experiment 3 and 14% for Experiments 1 and 2. Percentage mass loss for Experiments 4 and 5 were approximately 11% and 12%, respectively. This mass difference was also used in adjusting the volume for DIC calculations and estimating the moles of C and Mg in the residual solutions. Figs. 7 and 8 illustrate the elemental balances. Accuracy in C balance is limited by the considerations noted above, although a smaller residual of closure for Mg for the experiments confirm the measured amounts of formed precipitate. The results show a greater amount of carbonate formed for the experiments using small 20 μm bubbles and significantly reduced DIC at the end of these experiments, when compared to the experiments involving large 5 mm bubbles.

Two semibatch experiments were also completed in which 0.5 M $MgSO_4$ and 0.34 M $NaHCO_3$ solutions were fed to the reactor (temperature 30 °C) at fixed dosage rates of 1.1×10^{-5} mol s^{-1} and 2.3×10^{-5} mol s^{-1}, respectively, approximately equating to the stoichiometry of the precipitation reaction (cf. Eq. (1)). Dosage continued for almost a 2 h period, commencing at the point of precipitation. Both experiments involved the same initial chemical solution composition as the batch experiments, with one experiment catalysed by 0.25 μM CA, a lesser CA concentration than employed for the batch experiments. N_2 aeration (18 cm^3 s^{-1} using diffuser) continued upon reagent addition. For the experiment in which 0.25 μM CA was used in the initial batch, CA was also added to the $MgSO_4$ makeup solution to maintain the target concentration of 0.25 μM in the reactor. Fig. 9 depicts the pH trends and the measured concentration of CO_2 in the vented stream for each of the semibatch experiments.

Precipitation proceeds rapidly after the commencement of reagent addition, the concentration of CO_2 in the exhaust N_2 increases, and the solution pH declines approaching a more stable value. Lower CO_2 concentrations recorded for the CA experiment later during this period may be due to greater depletion of carbon from solution and elevated pH. Earlier recovery of pH, evident for the CA experiment, is an indicator of more rapid precipitation for the semibatch process involving reagent feed. There was also a noticeable delay in recovery of pH for the non-CA experiment on cessation of reagent feeds. It follows from pH measurements corroborated by micro GC data that, the incorporation of CA in the reacting system affords a faster rate of precipitation. A marked drop in flow through the diffuser (almost complete blockage at t = 2.5 h) for the experiment incorporating CA, confirms this observation. Additionally, the experiment employing CA generated a greater amount of precipitate for the same period of dosing; compare the amount of precipitates of 2.6 g with 2.1 g, for experiments

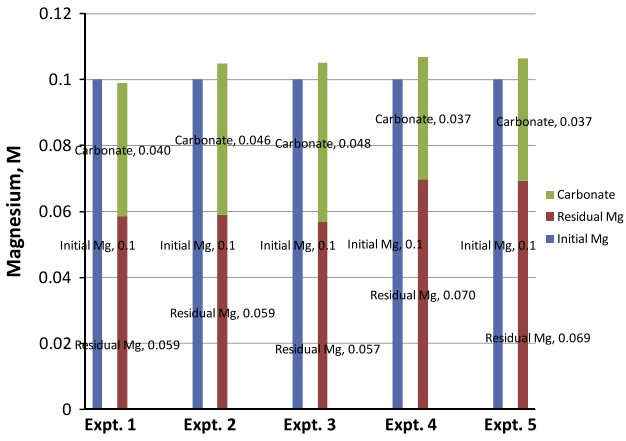

Fig. 7. Elemental magnesium balance for batch experiments.

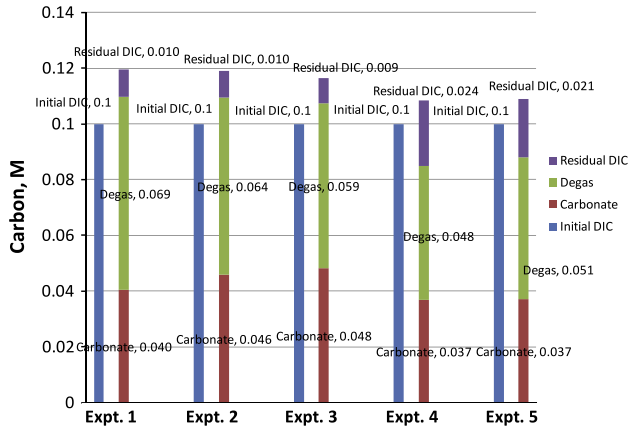

Fig. 8. Elemental carbon balance for batch experiments.

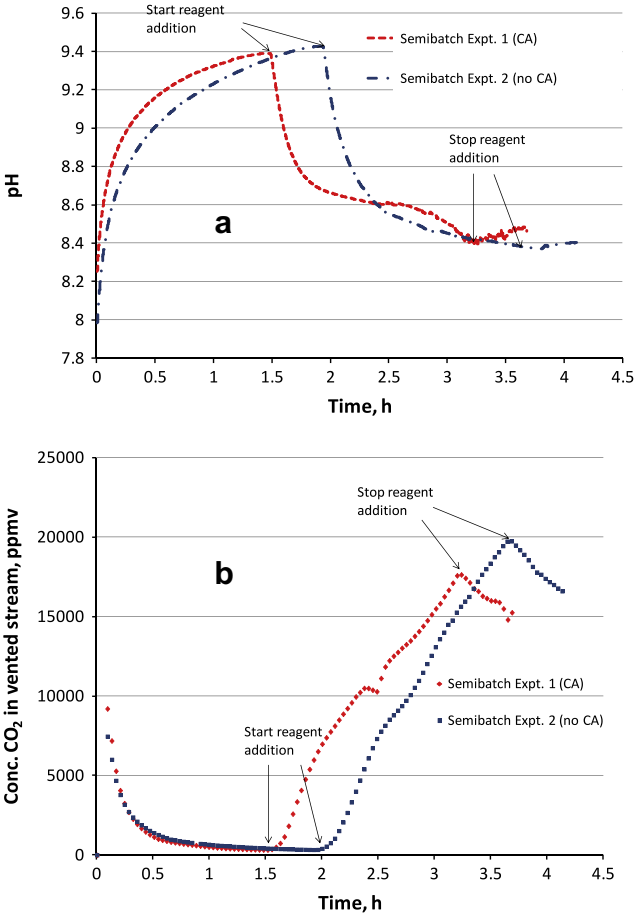

Fig. 9. The results of semibatch experiments show early recovery in pH for the CA catalysed run (a), and demonstrate increasing CO2 emissions subsequently to reagent addition (b).

with and without CA, respectively. Consequently, continuous recovery of precipitate could proceed at a greater rate with the inclusion of CA in the reacting system. Elemental balance was not considered appropriate because of large and rapid variation in vented flow rates over the course of the short duration experiments.

The process of degassing as a viable mechanism for mineral carbonation relies on the preparation of mineral solutions enriched in inorganic carbon. For batch operations the carbon to be sequestered must exist in the solution in the predominantly bicarbonate form to allow the solution to undergo degassing to precipitate carbonate. Such solutions are found in nature and can be produced in an engineering sense from processes mimicking natural formation of carbonates, such as those relying on enhanced interaction between meteoric water and pulverised ultramafic rocks.

For this work, we have considered batch and semibatch reactor configurations. These options or indeed a continuous reactor configuration may be best suited to large-scale degassing reactors. The essential feature of these reactor options is that CO_2 degassing provides the means of initial alkalisation, and a sufficiently alkalised state is maintained within the system by the continued evasion of CO_2 from the solution by the aeration medium. The alkalised system state is achieved without need for application of alkalinity which is energy intensive to produce (e.g., NaOH). In either a batch, semibatch or continuous process, the rate of precipitation is strongly dependent on the rate at which CO_2 is removed from the solution through aeration.

The degree of alkalisation achieved through degassing, necessary for precipitation, depends on the buffering capacity of the system. For example, the extent to which CO_2 needs to be removed from the system in order to create a supersaturation for nesquehonite of 5 decreases from 29% of initial solution DIC for a 0.1 $NaHCO_3$/0.1 M $MgSO_4$ solution to 17% of solution DIC for a 0.2 $NaHCO_3$/0.1 M $MgSO_4$ solution. The amount of carbonate produced per mole of CO_2 degassed also increases with increasingly DIC concentrated solutions. Consequently, the overall efficiency of the process can be increased significantly by using more concentrated solutions.

The precipitation of nesquehonite proceeds with a fixed stoichiometry (cf. Eq. 1). As a consequence, the solutions used in the reactor should comprise electrolytes with the overall C to Mg ratio of 2:1, for the most efficient precipitation of nesquehonite. Dissolution of pulverised ultramafic rocks (such as serpentinites) by carbonic acid is ideal, as it generates leachate of this molar ratio. The dissolution of this mineral source in its natural state using carbonic acid is limited (Oskierski et al., 2013). Using thermally conditioned serpentinites prepared with optimised heating strategies can significantly enhance dissolution (Balucan and Dlugogorski, 2013; Hariharan et al., 2013). Kinetic modelling allows for optimisation of degassing reactor processes. These considerations are a focus of ongoing research.

4. Conclusions

In this study, we have demonstrated the accelerated degassing of bicarbonate solutions by small bubbles and the catalytic effect of CA in enhancing rates of CO_2 degassing. The degassing and precipitation processes proceed in three phases, involving (i) alkalisation of the solution, appearance of supersaturation, and nuclei growth accompanying onset of carbonate precipitation, (ii) nesquehonite precipitation marked by pH decrease to the point that limits further precipitation, and (iii) subsequent alkalisation of the solution and approach to a steady state, involving stabilisation of pH and transfer of CO_2 from the local atmosphere to the system and concurrent removal of CO_2 from the solution by N_2 bubbles. For a practical application to large-scale CO_2 storage in nesquehonite, it should be possible to adopt the present process to operate large scale degassing reactions in batch, semibatch or flow configuration.

Acknowledgements

We thank Mr. H. Oskierski and Ms. M. Ghoorah of the University of Newcastle for completing XRPD analyses of the minerals precipitated in this study. T.K. Oliver thanks the University of Newcastle for the postgraduate research scholarship.

References

Balucan, R.D., Dlugogorski, B.Z., 2013. Thermal activation of antigorite for mineralization of CO_2. Environmental Science and Technology 47 (1), 182–190.

Berger, R., Libby, W.F., 1969. Equilibration of atmospheric carbon dioxide with sea water: possible enzymatic control of the rate. Science 164, 1395–1397.

Chou, L., Garrels, R.M., Wollast, R., 1989. Comparative study of the kinetics and mechanisms of dissolution of carbonate minerals. Chemical Geology 78 (3–4), 269–282.

Dreybrodt, W., Eisenlohr, L., Madry, B., Ringer, S., 1997. Precipitation kinetics of calcite in the system $CaCO_3$–H_2O–CO_2: The conversion to CO_2 by the slow process $H^+ + HCO_3^- \rightarrow CO_2 + H_2O$ as a rate limiting step. Geochimica et Cosmochimica Acta 61 (18), 3897–3904.

Dreybrodt, W., 2004. Dissolution: carbonate rocks. In: Gunn, J. (Ed.), Encyclopaedia of Cave and Karst Science. Routledge Taylor & Francis Group, New York, pp. 295–298.

Emmanuel, S., Ague, J.J., 2011. Impact of nano-size weathering products on the dissolution rates of primary minerals. Chemical Geology 282, 11–18.

Gavis, J., Ferguson, J.F., 1975. Kinetics of carbon dioxide uptake by phytoplankton at high pH. Limnology and Oceanography 20 (2), 211–221.

Hariharan, S., Werner, M., Zingaretti, D., Baciocchi, R., Mazzotti, M., 2013. Dissolution kinetics of thermally activated serpentine under flue gas atmosphere. 4th International Conference on Accelerated Carbonation for Environmental and Materials Engineering. Leuven, Belgium.

Helgeson, H., 1988. PRONS Data base. In: Johnson, J.W., Oelkers, E.H., Helgeson, H. (Eds.). University of California, Berkeley (SUPCRT92).

Johnson, M.T., 2010. A numerical scheme to calculate temperature and salinity dependent air-water transfer velocities for any gas. Ocean Science Discuss 7 (1), 251–290.

Koutsoukos, P.G., Kofina, A.N., Kanellopoulou, D.G., 2007. Solubility of salts in water: key issue for crystal growth and dissolution processes. Chem. Inform. 38 (40).

Liu, N., Bond, G.M., Abel, A., McPherson, B.J., Stringer, J., 2005. Biomimetic sequestration of CO_2 in carbonate form: role of produced waters and other brines. Fuel Processing Technology 86 (14–15), 1615–1625.

Liu, Y., Liu, Z., Zhang, J., He, Y., Sun, H., 2010. Experimental study on the utilization of DIC by oocystis solitaria wittr and its influence on the precipitation of calcium carbonate in karst and non-karst waters. Carbonates and Evaporites 25 (1), 21–26.

Liu, Z., 2001. Role of carbonic anhydrase as an activator in carbonate rock dissolution and its implication for atmospheric CO_2 sink. Acta Geologica Sinica - English Edition 75 (3), 275–278.

Mahinpey, N., Asghari, K., Mirjafari, P., 2011. Biological sequestration of carbon dioxide in geological formations. Chemical Engineering Research and Design 89 (9), 1873–1878.

Oskierski, H.C., Dlugogorski, B.Z., Jacobsen, G., 2013. Sequestration of atmospheric CO_2 in a weathering-derived, serpentinite-hosted magnesite deposit: ^{14}C tracing of carbon sources and age constraints for a refined genetic model. Geochimica et Cosmochimica Acta 122, 226–246.

Parkhurst, D.L.A., Appelo, C.A.J., 1999. User's guide to PHREEQC (Version 2) – a computer program for speciation, and inverse geochemical calculations. Geological Survey Water-Resources Investigations Report, US, 99–4259.

Pentecost, A., 2005. Travertine. Springer-Verlag, Heidelberg.

Plummer, L.N., Wigley, T.M.L., Parkhurst, D.L., 1978. The kinetics of calcite dissolution in CO_2-water systems at 5–60 °C and 0.0–1.0 atm CO_2. American Journal of Science 278, 179–216.

Söhnel, O., Mullin, J.W., 1988. Interpretation of crystallization induction periods. Journal of Colloid and Interface Science 123 (1), 43–50.

Sondi, I., Mladen, J., 2010. Whiting events and the formation of aragonite in mediterranean karstic marine lakes: new evidence on its biologically induced inorganic origin. Sedimentology 57 (1), 85–95.

Stumm, W.M., Morgan, J.J., 1996. Aquatic Chemistry, Chemical Equilibria in Natural Waters, third ed. J. Wiley and Sons Inc., New York.

Wolf-Gladrow, D., Riebesell, U., 1997. Diffusion and reactions in the vicinity of plankton: a refined model for inorganic carbon transport. Marine Chemistry 59 (1–2), 17–34.

Zeebe, R.E., Wolf-Gladrow, D., 2001. CO2 in Seawater: Equilibrium, Kinetics, Isotopes, third ed. Elsevier, Amsterdam.